PNAS RESEARCH ARTICLE | PSYCHOLOGICAL AND COGNITIVE SCIENCES NEUROSCIENCE

Morphological similarity of amygdala-ventral prefrontal pathways represents trait anxiety in younger and older adults

Wonyoung Kim[a] and M. Justin Kim[a,b,1]

Edited by Marcus Raichle, Mallinckrodt Institute of Radiology and Department of Neurology, Washington University School of Medicine, St. Louis, MO; received March 24, 2022; accepted August 2, 2022

Stronger amygdala-ventral prefrontal white matter connectivity has been associated with lower trait anxiety, possibly reflecting an increased capacity for efficient communication between the two regions. However, there are also reports arguing against this brain–anxiety association. To address these inconsistencies in the literature, we tested the possibility that idiosyncratic tract morphology may account for meaningful individual differences in trait anxiety, even among those with comparable microstructural integrity. Here, we adopted intersubject representational similarity analysis, an analytic framework that captures multivariate patterns of similarity, to analyze the morphological similarity of amygdala-ventral prefrontal pathways. Data drawn from the Leipzig Study for Mind–Body-Emotion Interactions dataset showed that younger adults (20 to 35 y of age) with low trait anxiety, in contrast to trait-anxious individuals, had consistently similar morphological configurations in their left amygdala-ventral prefrontal pathways. Additional tests on an independent sample of older adults (60 to 75 y of age) validated this finding. Our study reveals a generalizable pattern of brain–anxiety association that is embedded within the shared geometries between fiber tract morphology and trait anxiety data.

diffusion-weighted imaging | amygdala | prefrontal cortex | trait anxiety | representational similarity

Decades of research on the neurobiological basis of anxiety have consistently highlighted the central role of a corticolimbic circuit featuring the amygdala (1, 2) and the medial prefrontal cortex (PFC) (3, 4) as its primary components. While earlier research focused on elucidating the role of discrete brain regions in the generation and regulation of anxious states, an increasing number of studies examined their interconnected network, most notably the amygdala-ventral PFC circuitry (5–7). Emphasis on such circuit- and network-level analyses has contributed to a deeper understanding of the neurobiological basis of anxiety in both human and nonhuman animal research (8–11).

Inspired by rodent models of anxiety showing the importance of medial PFC communication to the amygdala for inhibiting learned fear responses (12), and anatomical tracing studies in monkeys delineating the reciprocal connectivity between the amygdala and various regions of the PFC (13), human neuroimaging studies utilized diffusion magnetic resonance imaging (dMRI) to noninvasively model amygdala-PFC white matter fiber tracts in the brain (14). An early dMRI study suggested an inverse association between the structural connectivity of the amygdala-ventral PFC pathways and self-reported levels of trait anxiety in healthy younger adults, such that trait-anxious individuals exhibited weaker connectivity (15). This pattern of brain–anxiety association was soon corroborated by findings from pathological anxiety, including social anxiety disorder (16, 17) and generalized anxiety disorder (18, 19), wherein the clinically diagnosed groups showed decreased structural connectivity of amygdala-ventral PFC pathways. These findings collectively suggest that weakened structural connectivity may be capturing a reduced capacity for efficient communication between the amygdala and ventral PFC in heightened anxiety (6). The perspective that efficient amygdala-PFC cross-talk leading to beneficial emotional outcomes is consistent with recent dMRI studies that show stronger microstructural integrity of amygdala-ventral PFC pathways facilitating better recovery from negative emotions (20), amygdala habituation to fearful faces (21), and top-down emotion regulation (22, 23).

While further evidence supporting the inverse association between amygdala-ventral PFC structural connectivity and trait anxiety in healthy individuals have accumulated from multiple research groups (23–26), comparison of available studies has been inconsistent (27–29). Age differences across study samples have been suggested to be one plausible reason for the discrepancy, as most earlier work is based on younger adults, while dMRI-derived connectivity measurements are heavily impacted by aging (30) and the amygdala-PFC pathway is among the slowest to reach maturity (31). Still, age differences alone do

Significance

Trait-anxious individuals, who are predisposed to experience anxiety in a wide range of situations, are at risk for anxiety disorders. Here, we combined intersubject representational similarity analysis and white matter tract morphology to explain individual differences in trait anxiety. First, the amygdala-prefrontal tract was defined using diffusion MRI data. As these tracts exhibit different shapes and sizes across individuals, we introduced the concept of "canvas space," a common space on which idiosyncratic tracts could be compared. Our analysis revealed that trait-anxious younger adults had more dissimilar tract morphology across individuals. This finding was validated in an independent sample of older adults, revealing a generalizable pattern that is embedded within the shared geometries between tract morphology and trait anxiety.

Author affiliations: [a]Department of Psychology, Sungkyunkwan University, Seoul 03063, South Korea; and [b]Center for Neuroscience Imaging Research, Institute for Basic Science, Sungkyunkwan University, Suwon 16419, South Korea

Author contributions: W.K. and M.J.K. designed research, performed research, analyzed data, and wrote the paper.

The authors declare no competing interest.

This article is a PNAS Direct Submission.

[1]To whom correspondence may be addressed. Email: minuekim@skku.edu.

This article contains supporting information online at http://www.pnas.org/lookup/suppl/doi:10.1073/pnas.2205162119/-/DCSupplemental.

Published October 10, 2022.

not fully explain the mixed findings in the literature, and thus there was a need to reconsider the strategy we have typically employed when mapping individual differences in trait anxiety onto the structural connectivity of the brain (i.e., simple correlations between trait anxiety and dMRI-derived metrics, such as fractional anisotropy [FA], averaged across entire fiber tracts).

To address this, we adopted intersubject representational similarity analysis (IS-RSA), an analytic framework that captures multivariate patterns of similarity (32), to analyze the morphological similarity of amygdala-ventral prefrontal pathways and its association with trait anxiety. In IS-RSA, pairwise distance matrices for brain data (e.g., amygdala-ventral PFC tract characteristics) and behavioral data (e.g., trait anxiety) are computed. Then, the geometry of the brain and behavioral matrices are compared using a correlation between similarity matrices (33). There are two notable advantages using IS-RSA over traditional methods. First, IS-RSA circumvents the need to directly associate two physically distinct quantities and instead uses second-order statistics to compare the geometries of brain data with behavioral data (34). Second, different models for similarity metrics (e.g., nearest neighbor, Anna Karenina [AnnaK]) allow flexibility in generating representational similarity matrices based on plausible brain–behavior associations (32).

We reasoned that if low scores represent "better" and high scores "worse" on the trait anxiety scale (35), then the morphological similarity of amygdala-ventral PFC tracts between individuals would decrease as trait anxiety scores increase. This is because while higher trait anxiety may be reflective of an altered state of amygdala-ventral PFC pathways (6), the pattern of such alterations would likely be nonuniform across individuals (i.e., different locations along the tract may be altered on an individual-by-individual basis). For this reason, we chose to assess morphological similarity instead of microstructural integrity averaged across tracts, as the former is sensitive to regional alterations along the amygdala-ventral PFC pathways. To this end, we tested the prediction that amygdala-ventral PFC tract morphology would be more similar in younger adults (20 to 35 y of age) with low trait anxiety, but more dissimilar in trait-anxious individuals. Then, we sought to externally validate the results in a sample of older adults (60 to 75 y of age) to examine the possible effects of aging on such brain–anxiety associations.

Results

IS-RSA. Amygdala-ventral PFC tracts at slice-level thresholds of 0%, 5%, and 10% were first visually inspected to check for false positives while also preserving the fine-grained tracts near the ventral PFC. Biologically implausible voxels were prevalent at the 0% threshold level, while voxels were excluded to the point where there were noticeable disconnections in the main tracts at the 10% threshold level (Fig. 1). Amygdala-ventral PFC tract images with the three levels of thresholds were then each transformed into amygdala-ventral PFC tract-morphology dissimilarity matrices by generating a "canvas space"—a common space on which idiosyncratic tracts could be compared against each other (*Materials and Methods* and Fig. 2)—resulting in three matrices per individual. As tests using these three matrices resulted in practically identical results, presumably because the effects were largely driven by voxels with high streamline counts (i.e., number of connections derived from probabilistic tractography), the results using the slice-level threshold of 5% are reported.

The Mantel test, which is a nonparametric test of significance where the rows and columns of one of the matrices are permuted to derive a null distribution of correlation values, was used to assess the Spearman rank correlation between the dissimilarity matrices (33). Mantel tests revealed that the left amygdala-ventral PFC tract-morphology dissimilarity matrix was significantly correlated with the trait-anxiety dissimilarity matrix ($P = 0.036$). However, the right amygdala-ventral PFC tract-morphology dissimilarity matrix was not correlated with the trait-anxiety dissimilarity matrix ($P = 0.622$). Mantel correlogram, a visualization technique that illustrates the more intricate pattern of correspondence between two matrices based on distance classes (33, 36, 37), showed that pairs with similarly low trait anxiety had a positive correspondence in the left amygdala-ventral PFC tract morphology (Fig. 3*A*).

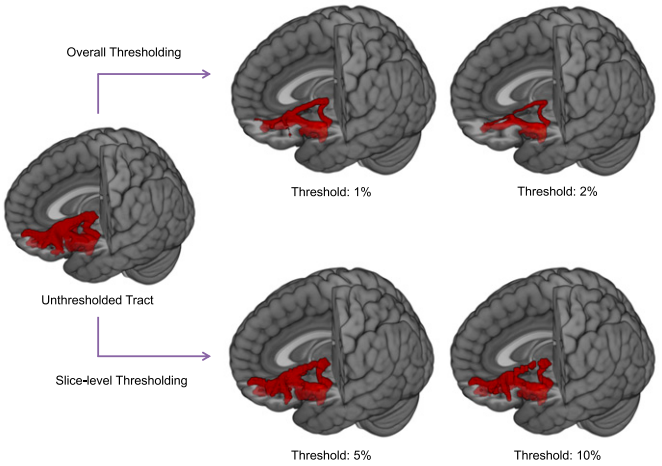

Fig. 1. Selection of thresholding schemes for amygdala-ventral PFC tracts. Resulting tracts from probabilistic tractography require an adequate thresholding scheme to minimize false positives. When thresholding at the tract level, finer tracts near the PFC are lost because streamline counts are disproportionately higher around the amygdala. On the other hand, when thresholding at the slice level, false positives are controlled while also preserving the finer tracts near the PFC. As 10% thresholding yielded visibly disconnected tracts, 5% slice-level thresholding was chosen for reporting results, although the results of the analyses remained virtually unchanged following thresholding schemes varying in percentage.

Tests on the older adult sample also depicted a significant correlation between the trait-anxiety dissimilarity matrix and the left amygdala-ventral PFC tract-morphology dissimilarity matrix ($P = 0.018$), but not the right amygdala-ventral PFC tract-morphology dissimilarity matrix ($P = 0.689$). A Mantel correlogram in the older adult sample showed a pattern of correspondence analogous to that of the younger adult sample (Fig. 3*C*). Results from the combined sample of younger and older adults remained consistent, such that the left amygdala-ventral PFC tract-morphology dissimilarity matrix was significantly correlated with the trait-anxiety dissimilarity matrix ($P = 0.00037$) (*SI Appendix*, Fig. S1).

Control Analyses. A total of 11 sets of control analyses were performed to explore potential alternative explanations of the main findings (*Materials and Methods*). 1) When tested for simple correlations, trait-anxiety score was not correlated with the mean tract integrity of the left ($P = 0.150$) or right ($P = 0.380$) amygdala-ventral PFC tracts. Results of the Mantel test using the mean tract integrity dissimilarity matrices were also not significant for the left ($P = 0.118$) or right ($P = 0.588$) amygdala-ventral PFC tracts (Fig. 4 *A* and *B*). 2) The trait-anxiety dissimilarity matrix was not correlated with the left ($P = 0.192$) or right ($P = 0.844$) regions of interest (ROIs) morphology dissimilarity matrices (Fig. 4 *C* and *D*). 3) The left amygdala-ventral PFC tract-morphology dissimilarity matrix matched in magnitude, which controlled the possible effect of difference in magnitude of

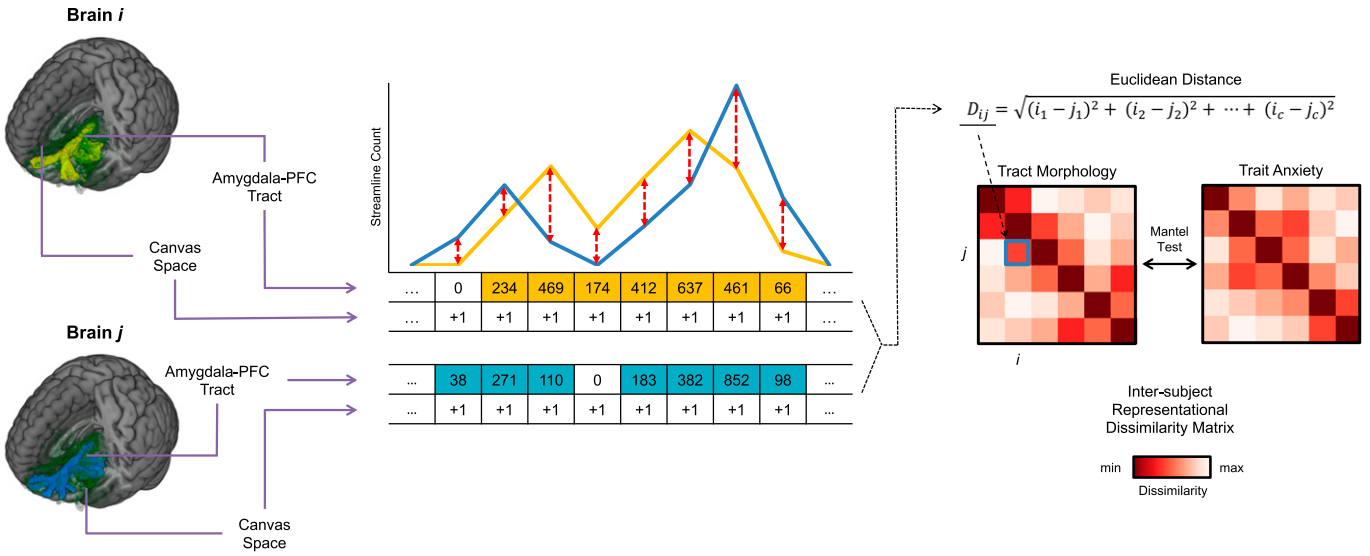

Fig. 2. Computation of amygdala-ventral PFC tract-morphology dissimilarity between individuals. Amygdala-ventral PFC tractography maps (marked as yellow or blue voxels) of two subjects, drawn on a common canvas space (marked as green voxels) comprised of *c* number of voxels, are vectorized and compared for dissimilarity using Euclidean distance. In vector form, streamline counts of voxels, arranged in the fixed order of varying *x-y-z* axes, are added on top of the canvas space values (i.e., one), yielding vectors with the uniform length of *c*. This procedure was repeated for all possible pairs of individuals, producing a 119 × 119 dissimilarity matrix for the younger adult sample and a 45 × 45 dissimilarity matrix for the older adult sample. Rendered brains are of selected subjects, but values in the vectors above were generated for illustrative purposes.

streamline counts, was still significantly correlated with the trait-anxiety dissimilarity matrix ($P = 0.026$). The right tract still showed no correspondence with trait anxiety when it was matched in magnitude before testing ($P = 0.783$) (Fig. 4 *E* and *F*). 4) Tract size dissimilarity matrix was not correlated with trait-anxiety dissimilarity matrix ($P = 0.103$). 5) Tract SD dissimilarity matrix was not correlated with trait-anxiety dissimilarity matrix ($P = 0.186$). 6) Dissimilarities in demographics were not correlated with dissimilarities in trait anxiety (age: $P = 0.499$; sex: $P = 0.618$). 7) Head motion dissimilarity matrix was not correlated with the trait-anxiety dissimilarity matrix ($P = 0.613$). 8) Tests using a control tract, which connects between the amygdala and occipital inferior lobe and corresponds to the inferior longitudinal fasciculus (ILF), yielded nonsignificant results in both the left ($P = 0.058$) and right ($P = 0.211$) hemispheres (Fig. 4 *G* and *H*). 9) Tests using an additional control tract that does not involve the amygdala (i.e., superior longitudinal fasciculus, SLF) also yielded nonsignificant results in both the left ($P = 0.456$) and right ($P = 0.926$) hemispheres (Fig. 4 *I* and *J*). Varying slice-level thresholds were also implemented on the control tract, and the results from the tract thresholded at 5% were used because there was no noticeable divergence in results of the three levels of thresholds. 10) When considered separately, neither tracts connecting the amygdala with the ventromedial PFC (vmPFC) nor orbitofrontal cortex (OFC) were significantly associated with trait-anxiety dissimilarity matrix ($P = 0.13$ and $P = 0.29$, respectively). 11) Amygdala-ventral PFC tract-morphology dissimilarity matrix was not correlated with the negative-affect dissimilarity matrix (left: $P = 0.789$; right: $P = 0.443$) (Fig. 4 *K* and *L*). When formally tested with reciprocal causal modeling (RCM), which is a method that allows model comparison based on Mantel tests, the amygdala-ventral PFC tract morphology model ($r = 0.15$) outperformed competing models using mean tract integrity, ROI morphology, tract size, tract SD, age, sex, and head motion in explaining trait anxiety (all other rs < 0.07) (*SI Appendix*, Table S1). The amygdala-ventral PFC tract morphology model ($r = 0.13$) also outperformed ILF and SLF (all rs < 0.11) control tracts (*SI Appendix*, Table S2). Finally, the amygdala-ventral PFC tract morphology was better explained by trait anxiety ($r = 0.11$) than general negative affect ($r = 0.02$) (*SI Appendix*, Table S3).

The same set of control analyses were carried out on the older adult sample (Fig. 5). Tests using mean tract integrity yielded nonsignificant results both for the simple correlations (left: $P = 0.484$; right: $P = 0.350$) and for the Mantel tests (left: $P = 0.744$; right: $P = 0.954$) (Fig. 5 *A* and *B*). Trait-anxiety dissimilarity matrix was not correlated with the left ($P = 0.795$) or right ($P = 0.589$) ROI morphology dissimilarity matrices (Fig. 5 *C* and *D*). The left amygdala-ventral PFC tract-morphology dissimilarity matrix was correlated with the trait-anxiety dissimilarity matrix even after matching in magnitude ($P = 0.041$), and the results of the right tract showed no change ($P = 0.424$) (Fig. 5 *E* and *F*). Trait-anxiety dissimilarity matrix was not correlated with tract size ($P = 0.848$). Correlation between tract SD and trait-anxiety dissimilarity matrices were significant ($P = 0.027$). While dissimilarity in sex was not correlated with trait-anxiety dissimilarity ($P = 0.587$), dissimilarity in age was correlated with trait-anxiety dissimilarity ($P = 0.008$). However, a post hoc partial Mantel test (38), controlling for the age dissimilarity matrix when testing for correlation between the left amygdala-ventral PFC tract-morphology dissimilarity matrix and the trait-anxiety dissimilarity matrix, remained significant ($P = 0.037$). Head motion dissimilarity was also not correlated with trait-anxiety dissimilarity ($P = 0.960$). Left ILF morphology dissimilarity matrix was correlated with the trait-anxiety dissimilarity matrix ($P = 0.023$), while the right ILF showed no correspondence with trait anxiety ($P = 0.124$) (Fig. 5 *G* and *H*). A partial Mantel test, which controlled for the variance in the left control tract-morphology dissimilarity matrix while testing for correlation between the left amygdala-ventral PFC tract-morphology dissimilarity matrix and the trait-anxiety dissimilarity matrix, was performed post hoc, as well as a Mantel test between the left amygdala-ventral PFC tract-morphology dissimilarity matrix and the left control tract-morphology dissimilarity matrix. After controlling for variance of the left control tract, the correlation was still significant ($P = 0.046$), and the matrices of the two tracts were not correlated with each other ($P = 0.182$). Similarly,

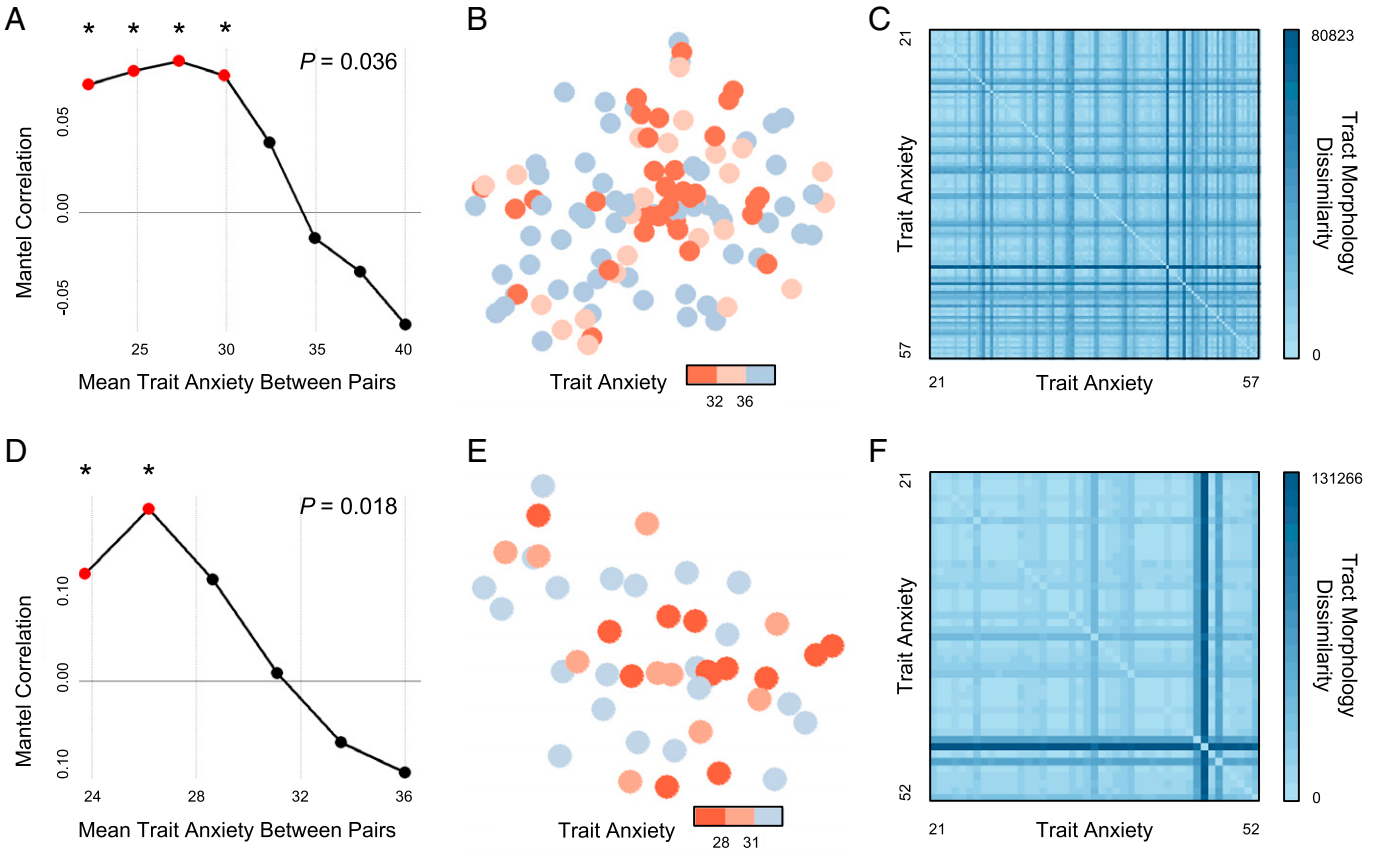

Fig. 3. Patterns of correlation between amygdala-ventral PFC tract-morphology dissimilarity and trait-anxiety dissimilarity. (*A*) Mantel correlogram showing positive correlation values between the left amygdala-ventral PFC tract-morphology dissimilarity and trait-anxiety dissimilarity, but only in pairs of individuals with comparably low trait anxiety. The *x* axis corresponds to the binned classes of the mean of the STAI-G-X2 trait anxiety measures between pairs of individuals, which is the measure of similarity in the "AnnaK" mean model. Each point of the graph is colored red and marked with * if the result of the specific class remains significant after correcting for multiple comparisons using false-discovery rate (FDR). (*B*) t-SNE, illustrating the multivariate distance between the amygdala-ventral PFC tract data of individuals by compressing them into a two-dimensional space. Color-coded using trait-anxiety scores with breaks at the first quartile and at the median, individuals show a similar pattern where individuals with similarly low trait anxiety are close to each other, whereas those high in trait anxiety are randomly dispersed. (*C*) Left amygdala-ventral PFC tract-morphology dissimilarity matrix showing greater similarity among individuals with low trait anxiety compared to those with high trait anxiety. Rows and columns are sorted by trait-anxiety levels. (*D*–*F*) Visualization of the older adult sample ($n = 45$), following the same procedure as the younger adult sample ($n = 119$).

the left SLF was significantly correlated with trait anxiety ($P = 0.031$), while the right SLF was not ($P = 0.645$) (Fig. 5 *I* and *J*). The same post hoc analyses described above for the left ILF showed that the amygdala-ventral PFC tract-morphology dissimilarity matrix was still significant after controlling for the variance of the left SLF ($P = 0.037$), and the two dissimilarity matrices were not correlated with each other ($P = 0.408$). Neither the amygdala-vmPFC or amygdala-OFC tracts were significantly associated with trait-anxiety dissimilarity matrix ($P = 0.11$ and $P = 0.14$, respectively). Excluding one participant without a Hamilton Depression Scale (HAM-D) score, principal component analysis (PCA) within the old sample revealed one factor ($-0.565 \times$ HAM-D; $-0.656 \times$ State-Trait Anxiety Inventory [STAI]; $-0.500 \times$ State-Trait Anger Expression Inventory [STAXI]) that accounted for 57.5% of variance common to these three measurements, and the resulting negative-affect dissimilarity matrix was not correlated with the amygdala-ventral PFC tract-morphology dissimilarity matrix (left: $P = 0.130$; right: $P = 0.926$) (Fig. 5 *K* and *L*).

RCM analysis showed that, similar to younger adults, the amygdala-ventral PFC tract morphology model ($r = 0.24$) outperformed competing models using mean tract integrity, ROI morphology, tract size, tract SD, age, sex, and head motion in explaining trait anxiety (all other rs < 0.2) (*SI Appendix*, Table S1). The amygdala-ventral PFC tract morphology model ($r = 0.25$) also outperformed the control tracts, although both the ILF ($r = 0.24$) and SLF ($r = 0.23$) were also correlated with trait anxiety, reflecting the Mantel test results above (*SI Appendix*, Table S2). Finally, the amygdala-ventral PFC tract morphology was better explained by trait anxiety ($r = 0.25$) than general negative affect ($r = -0.12$) (*SI Appendix*, Table S3).

Discussion

In the present study, probabilistic tractography maps of amygdala-ventral PFC white matter fiber tracts were compared using IS-RSA, which allowed investigation on individual differences in tract morphology, a feature previously regarded as noise in traditional methods that focus on mean tract integrity. Our results indicated that pairs of younger adults with comparably low trait anxiety were more similar to one another in their left amygdala-ventral PFC tract morphology, and this pattern was largely replicated in older adults. Such associations were not observed in the right hemisphere. Visual inspection of the results suggests that trait-anxious individuals tend to have increased variance in sections of the tract proximal to the amygdala (*SI Appendix*, Fig. S2). Overall, our study sheds light on the previously mixed findings regarding the relationship between the structural integrity of the amygdala-PFC pathways and trait anxiety by suggesting morphological features as a possible reason for such confounds.

Fig. 4. Summary of results from control analyses in younger adults. Mantel correlogram and t-SNE illustrating the patterns of correlation between bilateral mean tract integrity dissimilarity and trait-anxiety dissimilarity (*A* and *B*), bilateral ROIs morphology dissimilarity and trait-anxiety dissimilarity (*C* and *D*), bilateral magnitude-matched amygdala-ventral PFC tract dissimilarity and trait-anxiety dissimilarity (*E* and *F*), bilateral control tract (ILF, SLF) dissimilarity and trait-anxiety dissimilarity (*G–J*), and bilateral amygdala-ventral PFC tract-morphology dissimilarity and negative-affect dissimilarity (*K* and *L*). As anticipated, only the left magnitude-matched tract dissimilarity/trait-anxiety dissimilarity comparison followed the hypothesized pattern of correlation, similar to the main analysis. *$P < 0.05$ (FDR-corrected).

Analyzing the Morphology of the Amygdala-Ventral PFC Tract. Mean tract integrity is traditionally defined by averaging the FA values of voxels that are common in a certain percentage (e.g., 35% or 50%) of the tractography results of the participants (26, 27). By finding voxels that are reliable enough to consider as white matter pathways, this procedure ensures that the resulting FA value of white matter tracts is a valid estimation of microstructural integrity between two regions, but at the cost of disregarding the more intricate differences in tract morphology.

On the other hand, studying tract morphology in the standard univariate analytic framework of correlation and regression is obstructed by two factors: tracts of different individuals are heterogeneous in size and shape, and distinct morphological structures cannot be summarized into numeric values since their difference is more qualitative in nature than quantitative (i.e., tracts cannot be assigned "high" or "low" values based on their morphology other than oversimplified measures such total volume). We aimed to resolve the first issue by introducing the concept of canvas space, wherein all tractography images were compared in a common space without affecting the actual size of the tracts. The second issue, that each tract is qualitatively distinct, was circumvented by adopting IS-RSA, in which a measure of similarity in morphology between pairs of individuals, a measure that is quantifiable and hence adequate for statistical analyses, was employed.

Fig. 5. Summary of results from control analyses in older adults. Mantel correlogram and t-SNE illustrating the patterns of correlation between bilateral mean tract integrity dissimilarity and trait-anxiety dissimilarity (*A* and *B*), bilateral ROIs morphology dissimilarity and trait-anxiety dissimilarity (*C* and *D*), bilateral magnitude-matched amygdala-ventral PFC tract dissimilarity and trait-anxiety dissimilarity (*E* and *F*), bilateral control tract (ILF, SLF) dissimilarity and trait-anxiety dissimilarity (*G–J*), and bilateral amygdala-ventral PFC tract-morphology dissimilarity and negative-affect dissimilarity (*K* and *L*). Pattern of correlation between the left magnitude-matched tract dissimilarity and trait-anxiety dissimilarity followed the pattern of the main analysis as expected. Unlike the results of the younger adult sample, correlations between both left control tracts dissimilarity and trait-anxiety dissimilarity were statistically significant while also following the pattern of correlation of the main analysis. *$P < 0.05$ (FDR-corrected).

Importantly, we argue that the Euclidean distance between amygdala-ventral PFC tractography maps of different individuals reflects how morphologically dissimilar the tracts are at the whole-tract level. Previous studies that investigated individual differences in white matter morphology have done so in varying scales. Fixel-based analysis (FBA), for example, examines the fiber density and the fiber cross-section, which can be considered morphological features at the fiber level (39). While FBA has been shown to capture distinct features relevant to white matter morphology that the conventional diffusion tensor imaging (DTI)-based metrics such as FA cannot directly measure (40), it still necessitates summarizing the morphological characteristics across the whole tract, yielding one summarized score per tract. Local termination pattern analysis (LTPA), on the other hand, focuses on the local white matter connectivity patterns within given spatial constraints (e.g., fixed-size sphere), which measures morphology at the local level (41). Although ostensibly similar with our method in that it uses intersubject dissimilarities in streamline counts to compare white matter morphology between individuals, LTPA restricts its focus to regional variations of morphology, and is therefore agnostic of the functional significance of each white matter tract. Our method clearly defines the tract that is functionally of interest by carrying out probabilistic tractography between two ROIs and compares these tracts in their entirety through IS-RSA. In other words, our method is appropriate for analyzing how certain tracts of individuals morphologically differ from each other, which fit our goal of investigating the influence of idiosyncratic amygdala-ventral PFC white matter morphology in individual differences of trait anxiety.

Similar Amygdala-Ventral PFC Morphology Among Individuals with Low Trait Anxiety. The results of Mantel tests as well as visualization of data through Mantel correlograms and t-distributed stochastic neighbor embedding (t-SNE) imply that individuals low in trait anxiety share common morphologic characteristics in their left amygdala-ventral PFC white matter tracts, while the tracts of individuals high in trait anxiety are each distinct in their own way. This pattern suggests that a "healthy archetype" of amygdala-ventral PFC tract morphology exists, and atrophies occurring at different locations at different degrees are associated with higher trait anxiety. However, there are at least two possible sources of this ideal archetype: microstructural attributes and subregional connectivity patterns.

The first possibility is that microstructural attributes of the amygdala-ventral PFC tract could have been captured by our measures of morphology. To elaborate, microstructural characteristics of white matter tracts—such as the number of axons, diameter distribution, myelination, and membrane permeability—can influence tractography results (42), and dissimilarities in microstructure would likely result in morphologically dissimilar tracts. This would indicate that individuals with low trait anxiety have similar microstructural characteristics in their amygdala-ventral PFC tracts, a pattern that was not apparent when analyzing the dissimilarity of mean tract FA between individuals. Prior studies suggest that the amygdala-ventral PFC tract average FA, one of the various metrics of white matter microstructural integrity, is inversely correlated with trait anxiety (6, 23–26). However, individuals with the same mean tract FA can differ in their other microstructural attributes, and these differences may have contributed to contradictory results (27–29). One caveat of this interpretation is that our data are agnostic to the directionality of microstructural characteristics (e.g., strong or weak integrity) since it only indicates dissimilarity. Nevertheless, this possibility sheds light on previously mixed findings regarding the association between structural integrity of the amygdala-PFC pathways and trait anxiety, as a relationship between the microstructural features and trait anxiety only detectable through a multivariate approach may also be at work.

Second, our measure of tract morphology may represent different connections among distinct local regions within our ROIs. This is especially likely because the human amygdala and the ventral prefrontal ROIs that we used are each comprised of disparate subregions: the amygdala is an amalgam of at least 10 nuclei (43), and the ventral prefrontal ROIs were originally 5 divergent regions in the Automated Anatomical Labeling atlas (AAL3v1), although they were combined because they were previously found to have similar functional significance regarding their structural connections with the amygdala (26). Anatomically, locations within the OFC and vmPFC have a different ratio of input from and output to the amygdala, while subnuclei of the amygdala are segregated in their inhibitory and excitatory connections with the OFC and vmPFC (13, 44). Functional connectivity patterns of amygdala subregions were also found to be differentially disrupted in generalized anxiety disorder in adolescents and in adults (45–47). While pinpointing the exact mechanistic pathways that are associated with trait anxiety is outside the scope of this study, we believe that individual differences in the tract-level white matter morphology between the amygdala and ventral PFC could stem from differences in the fine-grained configurations in these subregional connections. In other words, low trait anxiety may be signified by a set of "right" connections between the amygdala and ventral PFC, a feature that could have been overlooked when analyzing the overall tract integrity between these regions.

Naturally, these two possible explanations are not mutually exclusive, and by no means exhaustive. Future studies could be designed to directly test these ideas and further expand on the results shown here. One potential route would be through employing higher resolution for imaging. In detail, 7T MRI data have recently been utilized in conducting tractography analyses for distinct nuclei of the amygdala (48), and analyzing the tract morphology of the more fine-grained white matter pathways related to these subregions would further enhance the resolution of our understanding toward the morphological organization of the amygdala-ventral PFC pathways and their functional roles. Another potentially fruitful line of research is adopting IS-RSA functional connectivity measures along with our IS-RSA tract morphology measures. Although the relationship between the amygdala-ventral PFC functional connectivity and trait anxiety is well documented (49, 50), it is possible that individual differences in a more detailed pattern of connectivity spanning multiple dimensions are at work, supported by the divergent morphology of the amygdala-ventral PFC white matter tracts. IS-RSA has been used to uncover more nuanced individual differences in functional interactions across the entire brain that are associated with behavior (32, 51, 52), and these same methods can theoretically be leveraged to investigate localized, yet still convoluted, patterns of functional connectivity between the amygdala and ventral PFC.

Exploration of Alternative Explanations. Eleven sets of control analyses on mean tract integrity, ROIs morphology, magnitude of tractography results, tract size, tract SD, two control tracts, demographics, head motion, and negative affect further demonstrated that the main results of this study were generally restricted to the association between amygdala-ventral PFC tract morphology and trait anxiety. These 11 control analyses can be summarized in

three categories: addressing covariates, testing the selectivity of brain measure, and testing the selectivity of behavior measure.

In detail, the amygdala-ventral PFC tract morphology measure that we chose was significantly related to trait anxiety, while other potential covariates were not. Probabilistic tractography has numerous potential factors that can confound the relationship between streamlines and true white matter tracts, such as anisotropy, length, width, curvature of tracts, as well as head motion and local signal-to-noise ratio (42, 53, 54). Tests using data of mean tract FA value, ROI morphology, magnitude of tractography results, tract size, tract SD, and head motion aimed to see if our main results on trait-anxiety dissimilarity were attributable to these confounding factors. Age and sex were also not significantly related to trait anxiety, which indicates that the main results were not attributable to age difference or sex difference within the sample. Furthermore, delineating the tract into amygdala-vmPFC and amygdala-OFC tracts no longer yielded significant associations between morphological similarity and trait anxiety. This suggests that, at least in the present dataset, both the vmPFC and OFC would need to be jointly considered for the definition of amygdala-ventral PFC tracts to capture its trait anxiety-related morphological characteristics. Future studies that probe the anatomical connections of the amygdala with different subregions of the PFC could further contribute to elucidating the nature of brain–anxiety association.

Notably, the tract between the amygdala and occipital inferior lobe, largely equivalent to the ILF, was selected as a control tract. Although the ILF, along with other major white matter tracts, has been previously implicated with social anxiety (55, 56) or generalized anxiety disorder (18, 57), it was theoretically not relevant to the amygdala-ventral PFC account of trait anxiety, and our results corroborated this hypothesis. An additional control analysis using the SLF, a tract that does not involve the amygdala, also yielded nonsignificant results. We therefore maintain that the amygdala-ventral PFC pathways are preferably related to trait anxiety, at least in younger adults.

Moreover, we tested the possibility of whether the effect of the amygdala-ventral PFC tract morphology measure is restricted to trait anxiety, as STAI measures may capture the general negative affect rather than trait anxiety per se (9, 58, 59), and as the amygdala-PFC white matter pathways also support general functions in regulating negative affect (20, 22, 23). Results indicated that trait anxiety is indeed selectively related to the morphological features of the amygdala-ventral PFC tract.

Overall, results from the control analyses and model comparisons consistently indicated that trait anxiety was best explained by the morphological similarity of the left amygdala-ventral PFC tract. While such associations were not observed in the right hemisphere, we are careful not to overinterpret the present findings as we did not directly test for laterality effects. Also, it is worth mentioning that some of the results from these control analyses (e.g., tract size, ILF morphology), despite not exceeding the significance threshold, may still be of interest for future studies as reciprocal causal modeling analyses suggest their relative importance in trait anxiety.

Validation in the Older Adult Sample. An external validation test was done on an older adult sample as well, which revealed a largely similar pattern of association between amygdala-ventral PFC tract morphology and trait anxiety. This implies that the aforementioned property of the "healthy archetype" of amygdala-ventral PFC tract morphology applies to older adults as well.

However, several unexpected effects were observed. First, age difference at three binned levels (ages 60 to 65 y, 65 to 60 y, and 70 to 75 y) evinced significant correlation with trait anxiety in the older adult sample. Such age effect in trait anxiety has also been recently reported where anxiety symptoms decreased at a much steeper rate for older adults than younger adults (60). Nevertheless, when controlling for the age dissimilarity, amygdala-ventral PFC tract-morphology dissimilarity was still correlated with trait-anxiety dissimilarity, meaning that the main result was not due to the age effect within the older adult sample. Furthermore, results from the combined sample of younger and older adults imply that the effect was present across age groups, despite age-related white matter differences, and that trait anxiety-related morphological properties of the amygdala-ventral PFC tract were preserved in aging.

Both left control tract (ILF, SLF) morphology was unexpectedly associated with trait anxiety, for which there are several possible explanations. First, it is possible that the morphology of the tract between the amygdala and occipital inferior lobe truly carries unique contributions to the individual differences in trait anxiety for older adults. Although this was not in line with our hypothesis, as the ILF may contribute to anxiety by abnormal perception of visual information in the environment in cases of domestic abuse survivors (61), unknown moderators that were presumably more prevalent in the older adult sample may have been at work. Second, in a scenario where older adults with low trait anxiety have uniformly higher structural integrity in the vicinity of the amygdala, all white matter tracts with the amygdala as a seed could be implicated with trait anxiety in our analytic framework. Although this is conceptually plausible as a distributed amygdala-centric network has been previously pointed out to be relevant to trait anxiety (25, 46), we could not directly test this with our methods because our measure of morphologic dissimilarity was at the whole tract level. However, since the left SLF, which doesn't involve the amygdala, also yielded a similar association with trait anxiety, it is possible that that trait anxiety may be reflected in the morphological features of white matter tracts in the left hemisphere more generally, at least in older adults. Of note, the possibility of the association between tract-morphology dissimilarity and trait-anxiety dissimilarity having a uniform effect in all white matter tracts across the whole brain is limited since our post hoc analysis demonstrated that there was no significant overlap in the contribution of each tract morphology to trait anxiety. Older adults with similar left amygdala-ventral PFC tract morphology did not share similar morphological features of either the left ILF or SLF, which is another indicator that these tracts have unique contributions to individual differences in trait anxiety among older adults.

In addition, the variance of the amygdala-ventral PFC tract morphology was associated with trait anxiety in older adults. This implies that the effect observed in the older adult sample is partially driven by dissimilarity in the distribution of streamline counts. Here, we are careful not to overinterpret these series of observations since the significant Mantel correlations found from the control analyses were unexpected findings from a relatively small study sample (i.e., less than half the size of younger adult sample). Nevertheless, these findings may provide testable hypotheses for future studies with an explicit focus on the aging brain.

In sum, the older adult sample has yielded a number of unexpected significant effects with regards to trait anxiety that deviated from the patterns seen in younger adults. Despite factors such as age, left ILF and SLF morphology, and tract SD being associated with trait anxiety in older adults, it is important to note a direct comparison of these competing models has consistently yielded the amygdala-ventral PFC tract morphology to be the best predictor of trait anxiety.

Limitations. Our study is not without limitations. First, the investigation of possible sex differences was limited. The moderating effect of sex was previously shown in the relationship between the amygdala-ventral PFC pathways and trait anxiety (26, 62). However, potential effects of sex could not be tested in detail in our study because Mantel tests are not ideal for capturing interaction between variables. Splitting the sample into males and females was also not ideal because females were underrepresented in our main analysis (84 males and 35 females) and splitting the sample would have resulted in significant imbalance in statistical power between the two groups. This gap in statistical power between males and females would also have been inflated in our analytic framework, as pairs of individuals ($84 \times 83 = 6{,}972$ for males; $35 \times 34 = 1{,}190$ for females) instead of individuals themselves would have been subjected to analyses. On the other hand, our control analysis confirmed that dissimilarity in sex did not drive the relationship between amygdala-ventral PFC dissimilarity and trait-anxiety dissimilarity, which implies that our results are likely generalizable to both males and females. That said, as males were especially overrepresented in the younger adult sample (>70%), the present results should still be interpreted with caution and the extent to which these findings may apply to females should be formally investigated in subsequent studies. Future investigations that aim to test the effects of sex in detail while using methods similar to ours are recommended to match the sample size between males and females.

Another shortcoming that needs mentioning is that the summary score of the German version of the Trait Scale of State-Trait Anxiety Inventory (STAI-G-X2) provided in the Max Planck Institute "Leipzig Study for Mind-Body-Emotion Interactions" (LEMON) dataset was used as a measure of trait anxiety, which inherently encompasses loss of item-wise data in individual differences. While using a trait-anxiety summary score is still useful as it facilitated comparison with previous findings, some IS-RSA studies that probed the multivariate item-wise dissimilarities among individuals found stronger evidence of coupling between brain similarity and behavior similarity than when using univariate summary score dissimilarities of the same measures (32, 51). It is thus possible that our results may have been attenuated, as there likely exist unexplored individual differences in specific items within the trait-anxiety assay. Nevertheless, the fact that our data resulted in significant findings despite this limitation may attest to the functional importance of the amygdala-ventral PFC pathways in trait anxiety.

Although we have performed a series of control analyses to rule out possible alternative explanations, there still are other factors to consider in future studies. These include the potential effect of angular resolution (i.e., number of diffusion directions) of dMRI data. Prior work demonstrated that brain–anxiety associations were not dependent on angular resolution of dMRI data when white matter FA values were used (26), but it remains an open question with regards to the morphological similarity of amygdala-ventral PFC tracts.

In addition, we reiterate that the unexpected results from the older adult sample should be interpreted with caution, due to the relatively smaller sample size and exploratory nature of the findings. That said, these observations provide a starting point for future studies to formally test the replicability of these effects in the aging brain. As an extension, applying the current approach on young children and adolescents would allow future studies to examine the extent to which trait anxiety may be manifested as morphological similarities in the amygdala-ventral PFC tract in the developing brain.

Finally, it should be noted that probabilistic tractography does not guarantee a fully truthful reconstruction of white matter tracts. Instead, it gives the best estimate of reliable pathways between two regions, which can be influenced by numerous factors other than tract morphology and are also prone to false positives (54, 63). That said, control analyses on mean tract FA value, ROI morphology, magnitude of tractography results, and head motion were conducted to ascertain that the main findings were attributable to individual differences in tract morphology. Furthermore, multiple levels of thresholds were employed to weed out the possibility of false positives driving the main results. Future studies should test if the association between tract morphology and behavior can be reproduced using other tractography pipelines, such as MRtrix3 that utilizes constrained spherical deconvolution (64), which has been shown to be more reliable than the traditional DTI measures (65), although technical prerequisites of this method, such as high angular resolution diffusion imaging data, must be addressed from the acquisition stage (66).

Conclusion. Our data showed that individuals with similar morphology of the amygdala-ventral PFC white matter tracts have similarly low trait anxiety, and this effect was found in both young and older adults. The main contribution of our study is that it opened new avenues for investigation on the more fine-grained features of the amygdala-PFC white matter tract beyond microstructural integrity, while also confirming the functional significance of this pathway in trait anxiety. This was made possible through adopting methods that explicate features of the white matter tract that are typically disregarded. Control analyses that explored alternative explanations for these findings along with validation analyses on a demographically divergent sample supplement the theoretical significance of the main findings. Future studies that investigate the association between the amygdala-PFC pathways and trait anxiety would benefit from taking into account the multivariate patterns that are possibly veiled behind the traditional univariate measures.

Materials and Methods

Participants. Data utilized in this study is part of the Max Planck Institute LEMON dataset (67) (*SI Appendix, Methods*). The dataset and its collection protocol are openly available to download at fcon_1000.projects.nitrc.org/indi/retro/MPI_LEMON.html. The LEMON study was in accordance with the World Medical Association Declaration of Helsinki and was approved by the Ethics Committee of the University of Leipzig (reference no. 154/13-ff).

Within the given sample, we primarily focused on younger adults (20 to 35 y of age) but carried out validation tests on older adults (60 to 75 y of age) as well. Of note, data utilized in this study were further screened based on current or history of psychiatric diagnoses [58 participants excluded, assessed through Standardized Clinical Interview for DSM-IV (68), or SCID-I (69)], missing structural or diffusion image data (9 participants excluded), and missing trait anxiety survey data (1 participant excluded).

The younger adult sample consisted of 119 healthy German-speaking participants (84 males, aged 20 to 35 y). The age of the participants was provided in 5-y-bins, and the number of participants in the age group of 20 to 25 y, 25 to 30 y, and 30 to 35 y were 62, 49, and 8, respectively. The older adult sample consisted of 45 healthy German-speaking participants (26 males, aged 60 to 75 y). The number of participants in the age group of 60 to 65 y, 65 to 70 y, and 70 to 75 y were 14, 18, and 13, respectively.

Image Acquisition. As the LEMON dataset followed a standardized procedure, we note that the following descriptions pertaining to image acquisition and preprocessing are described in the original paper (67) (*SI Appendix, Methods*).

Image Preprocessing and Quality Check. Preprocessed T1 MP2RAGE data provided by the authors of the LEMON dataset were used. In brief, the background of the uniform T1-weighted image was removed using CBS Tools (70). Then, the masked image was used for cortical surface reconstruction using FreeSurfer's recon-all (71, 72). A brain mask was created based on the FreeSurfer segmentation results, and diffeomorphic nonlinear registration of the ANTs SyN algorithm (73) was used to compute a spatial transformation between the individual's T1-weighted image and the Montreal Neurological Institute (MNI) 152 1-mm standard space. To remove identifying information from structural MRI scans, a defacing mask was created using CBS Tools (70) and then applied to all anatomical scans.

Preprocessing of diffusion-weighted images was done with FMRIB's Diffusion Toolbox (FDT) of FSL (FMRIB software library v6.0, https://fsl.fmrib.ox.ac.uk/fsl/fslwiki/) in the following order (74). First, *topup* was performed to correct for susceptibility-induced distortion, using two volumes with reversed phase encoding (75). Then, brain was extracted using BET (76). Eddy current distortions as well as possible artifacts from head motion were identified and corrected, using eddy with the *–repol* option (77, 78). Using DTIFIT on the cleaned diffusion-weighted images, whole-brain FA maps were constructed for each individual. FA maps were only used in the control analysis that adopts the traditional mean tract integrity approach.

Prior to further processing images, quality checks on diffusion images were performed using QUAD and SQUAD, the automated quality control tool in FSL (79). Results indicated that all participants fell under the exclusion threshold from previous literature, which was average volume-to-volume head motion of <3 mm or <5% of total outliers (80, 81). Visual inspection on the cleaned images confirmed this result, but because diffusion images are especially susceptible to head motion (82), head motion effects were further tested, as discussed in *Control Analyses*.

Probabilistic Tractography. First, ROIs were identified in the anatomical space of each individual. Bilateral amygdala were identified using FIRST, an automated segmentation tool for subcortical structures (83), then visually checked for any sign of errors. Bilateral orbitofrontal regions (labeled *OFCmed*, *OFCant*, *OFCpost*, and *OFClat*) and bilateral vmPFC (labeled *Frontal_Med_Orb*) were extracted from AAL3v1 in the MNI 152 standard space to be used as a combined ventral PFC ROI (84), as the amygdala heavily projects to and receive dense projections from these regions (13), and that the amygdala-ventral PFC tracts were previously demonstrated to be similarly associated with trait anxiety (23, 26). Following affine registration (FLIRT), nonlinear registration (FNIRT) was used to calculate the transformation between standard space and anatomical image (85), and the identified ventral PFC ROI was transformed into subject-specific anatomical space. Gray matter tissue was segmented using an automated segmentation tool (FAST) (86), and the resulting images were thresholded so that voxels of at least 35% probability of being assigned to gray matter remained. The PFC ROI was then masked with the thresholded gray matter images.

Second, *bedpostx* and *probtrackx2* were performed on the cleaned diffusion-weighted images to draw probabilistic tractography maps of the amygdala-ventral PFC white matter tracts in subject-specific anatomical space (87). Anatomically defined amygdala mask (identified via FIRST segmentation) was used as a seed mask, while atlas-based PFC mask was used as a target mask for tractography (Fig. 6*A*). The default 0.5-mm step length, 5,000 streamlines, and 2,000 steps were used. Then, the same algorithm was run, but with amygdala as the target and PFC as the seed. To reduce type I error rates, only the voxels that are present in the results of both tractography runs were retained for further analyses. Of note, exclusion masks were drawn between the left and right hemisphere in order to define ipsilateral tracts, and at the coronal plane posterior to amygdala at $y = -19$ (MNI) because we were only interested in direct amygdala-ventral prefrontal pathways that are anterior to amygdala. The voxel values of tractography maps were defined as the mean of the streamline values from the two runs of probabilistic tractography in the opposite direction.

Finally, tractography maps were thresholded to protect against false positives (63). Conventionally, thresholding is done at the tract level by identifying the voxel with the maximum count of streamlines, then excluding voxels with streamline count below a certain percentage of this voxel value (88–90). The current tractography results had greater concentration of streamlines near the amygdala compared to the streamlines near the PFC, thus a uniform threshold

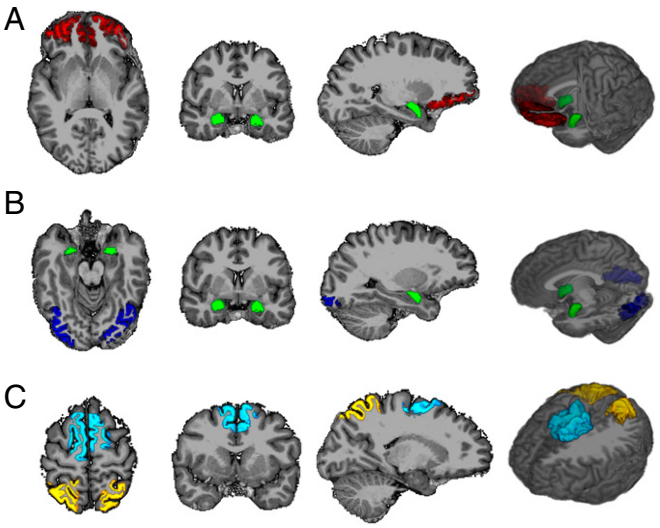

Fig. 6. Subject-specific ROIs for probabilistic tractography analysis. (*A*) ROIs used for the main analyses. The amygdala mask (green) and the prefrontal gray matter mask (red) were used as seed and target regions for probabilistic tractography. (*B*) ROIs used for the control tract analyses. The amygdala mask (green) and the occipital inferior lobe gray matter mask (blue) were used as seed and target regions for probabilistic tractography. (*C*) ROIs used for the control tract analyses. The superior parietal lobule mask (yellow) and the supplementary motor area mask (cyan) were used as seed and target regions for probabilistic tractography.

across the entire tract would disproportionally eliminate more voxels near the PFC than near the amygdala. Because individual differences in the fine-tuning of morphologic characteristics were of our primary interest, we sought to filter out false positives while also preserving the fine-grained tracts near the PFC. To this end, thresholding was done at the slice level (91). The detailed procedures are as follows: splitting the tractography maps into slices in the *y*-direction through *fslsplit*, then for each slice finding the maximum streamline value and excluding voxels under a certain percentage of this value, and then reconstructing tracts by merging the thresholded slices with *fslmerge*. Consequently, the maximum streamline values, and accordingly the absolute threshold values as well, were generally higher near the amygdala and lower near the PFC. By adopting slice-level thresholding, the gradient of streamline concentration along the *y* axis of the amygdala-ventral PFC tract was considered, preserving the fine-grained tracts near the PFC. Threshold percentage values of 0%, 5%, and 10% were each tested for further analyses.

IS-RSA. The amygdala-ventral PFC tract-morphology dissimilarity matrix between participants was constructed through the following procedure. First, individual probabilistic tractography maps were registered to the MNI 152 2-mm standard space. Crucially, even after registration into standard space, white matter tracts are inherently idiosyncratic in size; therefore, it is challenging to quantify a similarity metric between those of different individuals. To circumvent this issue, a "canvas space" was devised to add filler values to each tractography maps, yielding a common space on which idiosyncratic tracts could be compared against each other. We established the canvas space by adding all unthresholded tractography maps on one common image, and then binarizing, so that voxels that are included in at least one person's tractography result would have a value of one, while voxels that are not included in anyone's result would have a value of zero. Next, this canvas space image was then respectively added to the probabilistic tractography maps of individuals. This procedure ensured that upon vectorizing the images, tractography maps would be transformed into vectors with the same length, filled with values of one in unoccupied spaces, allowing comparison between these maps. Then, the voxels in each tractography maps were transformed into vectors using *fsl2ascii*, which takes images and yields voxel values in a fixed order based on *x-y-z* axes. Euclidean distance was derived from pairs of these vectors on a subject-by-subject basis (Fig. 2). In detail, the vectors stored the idiosyncratic morphology of tracts of individuals summarized as two dimensions of information: the tract streamline count of each voxel expressed as numeric values and the tract coordinates expressed as the order of numeric values. Euclidean distance

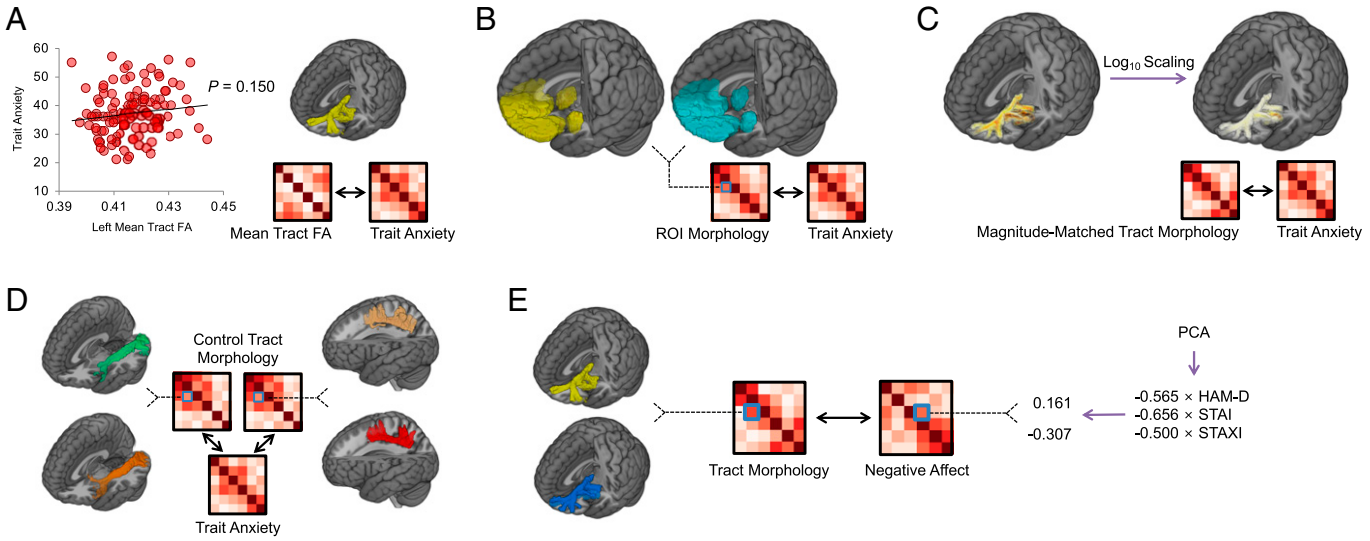

Fig. 7. Summary of control analyses procedures. (*A*) Mean tract FA values and trait anxiety scores were subject to simple correlations, following traditional methods. Furthermore, mean tract integrity dissimilarity matrices were compared against the tract-anxiety dissimilarity matrix. (*B*) Following the same procedures of the main analysis, idiosyncratic ROI morphology was used to construct ROI morphology dissimilarity matrices, which were then compared against the tract-anxiety dissimilarity matrix. (*C*) Tracts were matched in magnitude through $\log_{10}$ scaling of streamline values. The resulting magnitude-matched tract-morphology dissimilarity matrices were compared against the trait-anxiety dissimilarity matrix. (*D*) Using the ILF and SLF as control tracts, the same analyses were carried out. (*E*) Following PCA of depression symptom scores (HAM-D), trait-anger scores (STAXI), and trait-anxiety scores (STAI), negative-affect dissimilarity matrix was formed and compared against the amygdala-ventral PFC tract-morphology dissimilarity matrices. The pair of negative-affect scores shown here is from two representative subjects.

between two vectors would theoretically be minimized in cases where the streamline count and coordinates of tracts, and hence the numeric values and their order stored in vector form, are nearly identical between two individuals. On the other hand, distance would be maximized in cases where tracts of two individuals occupy the canvas space in a mutually exclusive way, resulting in high number of numeric values contrasted against the value of one (i.e., value of unoccupied space) instead of other numeric values. Importantly, because the canvas space values (i.e., one) were present among all vectors, the inclusion of these values had no effect in calculation of Euclidean distance. Finally, the Euclidean distance values between tracts of individuals were used to produce the amygdala-ventral PFC tract-morphology dissimilarity matrix.

Next, trait-anxiety dissimilarity matrix was formulated from the measured summary score of the STAI-G-X2 short version (35, 92). As per the methods described by Finn et al. (32), the AnnaK model was chosen to represent the similarity patterns of trait anxiety. The AnnaK model that we chose takes the mean value of trait-anxiety scores of the pairs of individuals as the metric of similarity. To elaborate, we predicted that the brain similarity between individuals with similarly low anxiety scores would be different from the brain similarity between individuals with similarly high anxiety scores, instead of assuming that anxiety similarity would be uniformly proportional to brain similarity. Although the AnnaK mean model can represent disproportionality on either side, since trait anxiety can be conceptualized as a measure of affective regulatory ability, we hypothesized that brain similarity would be higher among individuals with low anxiety than among individuals with high anxiety, much like working memory that was studied using the same model in the original paper (32). Importantly, other metrics (e.g., minimum) can be employed to address distinct forms of representation, but the arithmetic mean was used because it allows detection of effects in both directions with one test (32).

Finally, statistical analyses were carried out to compare the left and right amygdala-ventral PFC tract-morphology dissimilarity matrix with the anxiety dissimilarity matrix. The Mantel test, which is a nonparametric test of significance where the rows and columns of one of the matrices are permuted to derive a null distribution of correlation values, was used with 10,000 permutations to test the Spearman rank correlation between the two matrices (33). All manipulation of data and statistical analyses were done in R 4.0.5 (93) and its package 'vegan' (94).

The same procedure as described above has been implemented on the older adult sample as well to see if the results could be validated in a sample that has gone through significant white matter decline throughout the brain (95). For completeness, IS-RSA was performed with the combined sample of younger and older adults ($n = 164$) with the age dissimilarity matrix included as a covariate matrix in order to examine the effects of age on the main findings.

Control Analyses. We sought to conduct control analyses that explore potential alternative explanations of the observed results. Here we performed 11 additional analyses (*SI Appendix, Methods* and Fig. 7). A formal comparison among the main and control analyses were performed using RCM, with relative support to determine whether the amygdala-ventral PFC tract morphology model best explained trait anxiety (96, 97) (*SI Appendix, Methods*).

Data, Materials, and Software Availability. Anonymized data have been deposited in GitHub (https://doi.org/10.5281/zenodo.6381396) (98).

ACKNOWLEDGMENTS. We thank the original authors of the Max Planck Institute-LEMON dataset for their generosity in making it available for use. This research was supported by the National Research Foundation of Korea (NRF-2021R1F1A1045988).

1. M. Davis, P. J. Whalen, The amygdala: Vigilance and emotion. *Mol. Psychiatry* **6**, 13–34 (2001).
2. A. S. Fox, A. J. Shackman, The central extended amygdala in fear and anxiety: Closing the gap between mechanistic and neuroimaging research. *Neurosci. Lett.* **693**, 58–67 (2019).
3. S. J. Bishop, Neurocognitive mechanisms of anxiety: An integrative account. *Trends Cogn. Sci.* **11**, 307–316 (2007).
4. E. Likhtik, R. Paz, Amygdala-prefrontal interactions in (mal)adaptive learning. *Trends Neurosci.* **38**, 158–166 (2015).
5. C. A. Hartley, E. A. Phelps, Changing fear: The neurocircuitry of emotion regulation. *Neuropsychopharmacology* **35**, 136–146 (2010).
6. M. J. Kim *et al.*, The structural and functional connectivity of the amygdala: From normal emotion to pathological anxiety. *Behav. Brain Res.* **223**, 403–410 (2011).
7. G. J. Quirk, J. S. Beer, Prefrontal involvement in the regulation of emotion: Convergence of rat and human studies. *Curr. Opin. Neurobiol.* **16**, 723–727 (2006).
8. G. G. Calhoon, K. M. Tye, Resolving the neural circuits of anxiety. *Nat. Neurosci.* **18**, 1394–1404 (2015).
9. D. W. Grupe, J. B. Nitschke, Uncertainty and anticipation in anxiety: An integrated neurobiological and psychological perspective. *Nat. Rev. Neurosci.* **14**, 488–501 (2013).
10. M. M. Kenwood, N. H. Kalin, H. Barbas, The prefrontal cortex, pathological anxiety, and anxiety disorders. *Neuropsychopharmacology* **47**, 260–275 (2022).
11. M. R. Milad, G. J. Quirk, Fear extinction as a model for translational neuroscience: Ten years of progress. *Annu. Rev. Psychol.* **63**, 129–151 (2012).
12. M. R. Milad, G. J. Quirk, Neurons in medial prefrontal cortex signal memory for fear extinction. *Nature* **420**, 70–74 (2002).
13. H. T. Ghashghaei, C. C. Hilgetag, H. Barbas, Sequence of information processing for emotions based on the anatomic dialogue between prefrontal cortex and amygdala. *Neuroimage* **34**, 905–923 (2007).

14. H. Johansen-Berg *et al.*, Anatomical connectivity of the subgenual cingulate region targeted with deep brain stimulation for treatment-resistant depression. *Cereb. Cortex* **18**, 1374–1383 (2008).
15. M. J. Kim, P. J. Whalen, The structural integrity of an amygdala-prefrontal pathway predicts trait anxiety. *J. Neurosci.* **29**, 11614–11618 (2009).
16. V. Baur *et al.*, White matter alterations in social anxiety disorder. *J. Psychiatr. Res.* **45**, 1366–1372 (2011).
17. K. L. Phan *et al.*, Preliminary evidence of white matter abnormality in the uncinate fasciculus in generalized social anxiety disorder. *Biol. Psychiatry* **66**, 691–694 (2009).
18. J. M. Hettema *et al.*, Pilot multimodal twin imaging study of generalized anxiety disorder. *Depress. Anxiety* **29**, 202–209 (2012).
19. D. P. Tromp *et al.*, Reduced structural connectivity of a major frontolimbic pathway in generalized anxiety disorder. *Arch. Gen. Psychiatry* **69**, 925–934 (2012).
20. W. S. Pedersen *et al.*, Individual variation in white matter microstructure is related to better recovery from negative stimuli. *Emotion* **22**, 244–257 (2022).
21. T. C. Hein *et al.*, Amygdala habituation and uncinate fasciculus connectivity in adolescence: A multi-modal approach. *Neuroimage* **183**, 617–626 (2018).
22. T. C. d'Arbeloff *et al.*, Microstructural integrity of a pathway connecting the prefrontal cortex and amygdala moderates the association between cognitive reappraisal and negative emotions. *Emotion* **18**, 912–915 (2018).
23. A. S. Eden *et al.*, Emotion regulation and trait anxiety are predicted by the microstructure of fibers between amygdala and prefrontal cortex. *J. Neurosci.* **35**, 6020–6027 (2015).
24. N. A. J. De Witte, S. C. Mueller, White matter integrity in brain networks relevant to anxiety and depression: Evidence from the human connectome project dataset. *Brain Imaging Behav.* **11**, 1604–1615 (2017).
25. S. G. Greening, D. G. V. Mitchell, A network of amygdala connections predict individual differences in trait anxiety. *Hum. Brain Mapp.* **36**, 4819–4830 (2015).
26. M. J. Kim *et al.*, The inverse relationship between the microstructural variability of amygdala-prefrontal pathways and trait anxiety is moderated by sex. *Front. Syst. Neurosci.* **10**, 93 (2016).
27. D. Clewett, S. Bachman, M. Mather, Age-related reduced prefrontal-amygdala structural connectivity is associated with lower trait anxiety. *Neuropsychology* **28**, 631–642 (2014).
28. S. Modi *et al.*, Individual differences in trait anxiety are associated with white matter tract integrity in fornix and uncinate fasciculus: Preliminary evidence from a DTI based tractography study. *Behav. Brain Res.* **238**, 188–192 (2013).
29. C. Montag, M. Reuter, B. Weber, S. Markett, J. C. Schoene-Bake, Individual differences in trait anxiety are associated with white matter tract integrity in the left temporal lobe in healthy males but not females. *Neuroscience* **217**, 77–83 (2012).
30. S. W. Davis *et al.*, Assessing the effects of age on long white matter tracts using diffusion tensor tractography. *Neuroimage* **46**, 530–541 (2009).
31. C. Lebel, L. Walker, A. Leemans, L. Phillips, C. Beaulieu, Microstructural maturation of the human brain from childhood to adulthood. *Neuroimage* **40**, 1044–1055 (2008).
32. E. S. Finn *et al.*, Idiosynchrony: From shared responses to individual differences during naturalistic neuroimaging. *Neuroimage* **215**, 116828 (2020).
33. N. Mantel, The detection of disease clustering and a generalized regression approach. *Cancer Res.* **27**, 209–220 (1967).
34. N. Kriegeskorte, R. A. Kievit, Representational geometry: Integrating cognition, computation, and the brain. *Trends Cogn. Sci.* **17**, 401–412 (2013).
35. C. D. Spielberger, R. L. Gorsuch, R. E. Lushene, *STAI: Manual for the State-Trait Anxiety Inventory* (Consulting Psychologists Press, Palo Alto, CA, 1970).
36. N. L. Oden, R. R. Sokal, Directional autocorrelation: An extension of spatial correlograms to two dimensions. *Syst. Zool.* **35**, 608–617 (1986).
37. D. Borcard, P. Legendre, Is the Mantel correlogram powerful enough to be useful in ecological analysis? A simulation study. *Ecology* **93**, 1473–1481 (2012).
38. P. E. Smouse, J. C. Long, R. R. Sokal, Multiple regression and correlation extensions of the Mantel test of matrix correspondence. *Syst. Zool.* **35**, 627–632 (1986).
39. D. A. Raffelt *et al.*, Investigating white matter fibre density and morphology using fixel-based analysis. *Neuroimage* **144** (Pt A), 58–73 (2017).
40. D. Dimond *et al.*, Early childhood development of white matter fiber density and morphology. *Neuroimage* **210**, 116552 (2020).
41. M. Cieslak, S. T. Grafton, Local termination pattern analysis: A tool for comparing white matter morphology. *Brain Imaging Behav.* **8**, 292–299 (2014).
42. D. K. Jones, Challenges and limitations of quantifying brain connectivity in vivo with diffusion MRI. *Imaging Med.* **2**, 341 (2010).
43. P. Sah, E. S. Faber, M. Lopez De Armentia, J. Power, The amygdaloid complex: Anatomy and physiology. *Physiol. Rev.* **83**, 803–834 (2003).
44. R. D. Ray, D. H. Zald, Anatomical insights into the interaction of emotion and cognition in the prefrontal cortex. *Neurosci. Biobehav. Rev.* **36**, 479–501 (2012).
45. A. Etkin, K. E. Prater, A. F. Schatzberg, V. Menon, M. D. Greicius, Disrupted amygdalar subregion functional connectivity and evidence of a compensatory network in generalized anxiety disorder. *Arch. Gen. Psychiatry* **66**, 1361–1372 (2009).
46. A. K. Roy *et al.*, Intrinsic functional connectivity of amygdala-based networks in adolescent generalized anxiety disorder. *J. Am. Acad. Child Adolesc. Psychiatry* **52**, 290–299.e2 (2013).
47. C. Wang *et al.*, Anomalous static and dynamic functional connectivity of amygdala subregions in individuals with high trait anxiety. *Depress. Anxiety* **38**, 860–873 (2021).
48. S. S. G. Brown *et al.*, Ultra-high-resolution imaging of amygdala subnuclei structural connectivity in major depressive disorder. *Biol. Psychiatry Cogn. Neurosci. Neuroimaging* **5**, 184–193 (2020).
49. J. Bijsterbosch, S. Smith, S. J. Bishop, Functional connectivity under anticipation of shock: Correlates of trait anxious affect versus induced anxiety. *J. Cogn. Neurosci.* **27**, 1840–1853 (2015).
50. S. Delli Pizzi *et al.*, Functional and neurochemical interactions within the amygdala-medial prefrontal cortex circuit and their relevance to emotional processing. *Brain Struct. Funct.* **222**, 1267–1279 (2017).
51. P. A. Chen, E. Jolly, J. H. Cheong, L. J. Chang, Intersubject representational similarity analysis reveals individual variations in affective experience when watching erotic movies. *Neuroimage* **216**, 116851 (2020).
52. S. A. Rhoads *et al.*, Mapping neural activity patterns to contextualized fearful facial expressions onto callous-unemotional (CU) traits: Intersubject representational similarity analysis reveals less variation among high-CU adolescents. *Personal. Neurosci.* **3**, e12 (2020).
53. G. L. Baum *et al.*, The impact of in-scanner head motion on structural connectivity derived from diffusion MRI. *Neuroimage* **173**, 275–286 (2018).
54. D. K. Jones, T. R. Knösche, R. Turner, White matter integrity, fiber count, and other fallacies: The do's and don'ts of diffusion MRI. *Neuroimage* **73**, 239–254 (2013).
55. V. R. Steiger *et al.*, Pattern of structural brain changes in social anxiety disorder after cognitive behavioral group therapy: A longitudinal multimodal MRI study. *Mol. Psychiatry* **22**, 1164–1171 (2017).
56. S. Whitfield-Gabrieli *et al.*, Brain connectomics predict response to treatment in social anxiety disorder. *Mol. Psychiatry* **21**, 680–685 (2016).
57. M. Liao *et al.*, White matter abnormalities in adolescents with generalized anxiety disorder: A diffusion tensor imaging study. *BMC Psychiatry* **14**, 41 (2014).
58. A. Bados, J. Gómez-Benito, G. Balaguer, The state-trait anxiety inventory, trait version: Does it really measure anxiety? *J. Pers. Assess.* **92**, 560–567 (2010).
59. H. Caci, F. J. Baylé, C. Dossios, P. Robert, P. Boyer, The Spielberger Trait Anxiety Inventory measures more than anxiety. *Eur. Psychiatry* **18**, 394–400 (2003).
60. L. A. Rutter *et al.*, Emotion sensitivity and self-reported symptoms of generalized anxiety disorder across the lifespan: A population-based sample approach. *Brain Behav.* **9**, e01282 (2019).
61. J. Choi, B. Jeong, A. Polcari, M. L. Rohan, M. H. Teicher, Reduced fractional anisotropy in the visual limbic pathway of young adults witnessing domestic violence in childhood. *Neuroimage* **59**, 1071–1079 (2012).
62. C. A. Burghy *et al.*, Developmental pathways to amygdala-prefrontal function and internalizing symptoms in adolescence. *Nat. Neurosci.* **15**, 1736–1741 (2012).
63. T. Sarwar, K. Ramamohanarao, A. Zalesky, Mapping connectomes with diffusion MRI: Deterministic or probabilistic tractography? *Magn. Reson. Med.* **81**, 1368–1384 (2019).
64. J. D. Tournier, F. Calamante, A. Connelly, Robust determination of the fibre orientation distribution in diffusion MRI: Non-negativity constrained super-resolved spherical deconvolution. *Neuroimage* **35**, 1459–1472 (2007).
65. S. Farquharson *et al.*, White matter fiber tractography: Why we need to move beyond DTI. *J. Neurosurg.* **118**, 1367–1377 (2013).
66. J. D. Tournier *et al.*, MRtrix3: A fast, flexible and open software framework for medical image processing and visualisation. *Neuroimage* **202**, 116137 (2019).
67. A. Babayan *et al.*, A mind-brain-body dataset of MRI, EEG, cognition, emotion, and peripheral physiology in young and old adults. *Sci. Data* **6**, 180308 (2019).
68. H. Saß, H. U. Wittchen, M. Zaudig, *Diagnostisches und Statistisches Manual Psychischer Störungen-DSM-IV* (Hogrefe, Göttingen, 1996).
69. H. U. Wittchen, U. Wunderlich, S. Gruschwitz, M. Zaudig, *SKID I. Strukturiertes Klinisches Interview für DSM-IV. Achse I: Psychische Störungen. Interviewheft und Beurteilungsheft* (Hogrefe, 1997).
70. P. L. Bazin *et al.*, A computational framework for ultra-high resolution cortical segmentation at 7Tesla. *Neuroimage* **93**, 201–209 (2014).
71. A. M. Dale, B. Fischl, M. I. Sereno, Cortical surface-based analysis. I. Segmentation and surface reconstruction. *Neuroimage* **9**, 179–194 (1999).
72. B. Fischl, M. I. Sereno, A. M. Dale, Cortical surface-based analysis. II: Inflation, flattening, and a surface-based coordinate system. *Neuroimage* **9**, 195–207 (1999).
73. B. B. Avants *et al.*, A reproducible evaluation of ANTs similarity metric performance in brain image registration. *Neuroimage* **54**, 2033–2044 (2011).
74. M. Jenkinson, C. F. Beckmann, T. E. Behrens, M. W. Woolrich, S. M. Smith, FSL. *Neuroimage* **62**, 782–790 (2012).
75. J. L. Andersson, S. Skare, J. Ashburner, How to correct susceptibility distortions in spin-echo echo-planar images: Application to diffusion tensor imaging. *Neuroimage* **20**, 870–888 (2003).
76. S. M. Smith, Fast robust automated brain extraction. *Hum. Brain Mapp.* **17**, 143–155 (2002).
77. J. L. R. Andersson, M. S. Graham, E. Zsoldos, S. N. Sotiropoulos, Incorporating outlier detection and replacement into a non-parametric framework for movement and distortion correction of diffusion MR images. *Neuroimage* **141**, 556–572 (2016).
78. J. L. R. Andersson, S. N. Sotiropoulos, An integrated approach to correction for off-resonance effects and subject movement in diffusion MR imaging. *Neuroimage* **125**, 1063–1078 (2016).
79. M. Bastiani *et al.*, Automated quality control for within and between studies diffusion MRI data using a non-parametric framework for movement and distortion correction. *Neuroimage* **184**, 801–812 (2019).
80. H. Li *et al.*, Brainstem involvement in amyotrophic lateral sclerosis: A combined structural and diffusion tensor MRI analysis. *Front. Neurosci.* **15**, 675444 (2021).
81. H. Zheng *et al.*; Tulsa 1000 Investigators, Replicable association between human cytomegalovirus infection and reduced white matter fractional anisotropy in major depressive disorder. *Neuropsychopharmacology* **46**, 928–938 (2021).
82. A. Yendiki, K. Koldewyn, S. Kakunoori, N. Kanwisher, B. Fischl, Spurious group differences due to head motion in a diffusion MRI study. *Neuroimage* **88**, 79–90 (2014).
83. B. Patenaude, S. M. Smith, D. N. Kennedy, M. Jenkinson, A Bayesian model of shape and appearance for subcortical brain segmentation. *Neuroimage* **56**, 907–922 (2011).
84. E. T. Rolls, C. C. Huang, C. P. Lin, J. Feng, M. Joliot, Automated anatomical labelling atlas 3. *Neuroimage* **206**, 116189 (2020).
85. M. Jenkinson, P. Bannister, M. Brady, S. Smith, Improved optimization for the robust and accurate linear registration and motion correction of brain images. *Neuroimage* **17**, 825–841 (2002).
86. Y. Zhang, M. Brady, S. Smith, Segmentation of brain MR images through a hidden Markov random field model and the expectation-maximization algorithm. *IEEE Trans. Med. Imaging* **20**, 45–57 (2001).
87. T. E. Behrens, H. J. Berg, S. Jbabdi, M. F. Rushworth, M. W. Woolrich, Probabilistic diffusion tractography with multiple fibre orientations: What can we gain? *Neuroimage* **34**, 144–155 (2007).
88. J. D. Schaechter *et al.*, Microstructural status of ipsilesional and contralesional corticospinal tract correlates with motor skill in chronic stroke patients. *Hum. Brain Mapp.* **30**, 3461–3474 (2009).
89. R. Lindenberg, L. L. Zhu, T. Rüber, G. Schlaug, Predicting functional motor potential in chronic stroke patients using diffusion tensor imaging. *Hum. Brain Mapp.* **33**, 1040–1051 (2012).
90. R. Schulz *et al.*, Assessing the integrity of corticospinal pathways from primary and secondary cortical motor areas after stroke. *Stroke* **43**, 2248–2251 (2012).
91. D. B. Archer, D. E. Vaillancourt, S. A. Coombes, A template and probabilistic atlas of the human sensorimotor tracts using diffusion MRI. *Cereb. Cortex* **28**, 1685–1699 (2018).
92. L. Laux, P. Glanzmann, P. Schaffner, C. D. Spielberger, *Das State-Trait-Angstinventar* (Beltz Test GmbH., Weinheim, 1981).

93. R Core Team, R: A language and environment for statistical computing. (R Foundation for Statistical Computing, Vienna, Austria, 2021). https://www.R-project.org/. Accessed 10 September 2021.
94. Oksanen, J., et al. Package 'vegan'. Community ecology package, version, 2(9), 1-295 (2013). https://CRAN.R-project.org/package=vegan. Accessed 22 October 2021.
95. A. Z. Burzynska *et al.*, Age-related differences in white matter microstructure: Region-specific patterns of diffusivity. *Neuroimage* **49**, 2104–2112 (2010).
96. S. A. Cushman, T. N. Wasserman, E. L. Landguth, A. J. Shirk, Re-evaluating causal modeling with Mantel tests in landscape genetics. *Diversity (Basel)* **5**, 51–72 (2013).
97. A. J. Shirk, E. L. Landguth, S. A. Cushman, A comparison of regression methods for model selection in individual-based landscape genetic analysis. *Mol. Ecol. Resour.* **18**, 55–67 (2018).
98. W. Kim, M.J. Kim, Morphological similarity of amygdala-ventral prefrontal pathways represents trait anxiety in younger and older adults. GitHub. https://zenodo.org/record/6381396#.YzXCTHZBy3A. Deposited 24 March 2022.